communications biology

Article

https://doi.org/10.1038/s42003-024-06715-3

Functional analysis of *ESRP1/2* gene variants and *CTNND1* isoforms in orofacial cleft pathogenesis

Caroline Caetano da Silva[1,10], Claudio Macias Trevino[2,10], Jason Mitchell[3,10], Hemma Murali[4], Casey Tsimbal[1,5], Eileen Dalessandro[1], Shannon H. Carroll[1,5], Simren Kochhar[6], Sarah W. Curtis[6], Ching Hsun Eric Cheng[1], Feng Wang[7], Eric Kutschera[7], Russ P. Carstens[8], Yi Xing[4,7], Kai Wang[4], Elizabeth J. Leslie[6] & Eric C. Liao[1,2,5,9] ✉

Orofacial cleft (OFC) is a common human congenital anomaly. Epithelial-specific RNA splicing regulators *ESRP1* and *ESRP2* regulate craniofacial morphogenesis and their disruption result in OFC in zebrafish, mouse and humans. Using *esrp1/2* mutant zebrafish and murine Py2T cell line models, we functionally tested the pathogenicity of human *ESRP1/2* gene variants. We found that many variants predicted by in silico methods to be pathogenic were functionally benign. *Esrp1* also regulates the alternative splicing of *Ctnnd1* and these genes are co-expressed in the embryonic and oral epithelium. In fact, over-expression of *ctnnd1* is sufficient to rescue morphogenesis of epithelial-derived structures in *esrp1/2* zebrafish mutants. Additionally, we identified 13 *CTNND1* variants from genome sequencing of OFC cohorts, confirming *CTNND1* as a key gene in human OFC. This work highlights the importance of functional assessment of human gene variants and demonstrates the critical requirement of *Esrp-Ctnnd1* acting in the embryonic epithelium to regulate palatogenesis.

The study of orofacial cleft (OFC) has been foundational to genetic analysis of congenital anomalies. Craniofacial structural malformations are amenable to detailed phenotypic classification in large cohorts where genomic studies have been carried out to identify associated loci[1–8]. As whole-genome sequencing (WGS) strategies and technologies advance, a growing list of genes and gene variants associated with OFC are being cataloged[1,8–11]. These approaches have uncovered the critical role of many genes regulating the embryonic oral epithelium in palate formation and OFC pathogenesis, including: *TP63*, *IRF6*, *GRHL3*, *ESRP1/2*, *CTNND1*[12–24].

Because most cases of non-syndromic OFC occur sporadically, the pathogenicity of variants cannot be inferred or supported by segregation among affected family members. Therefore, determining the functional significance of gene variants remains challenging. Multiple in silico predictive algorithms such as SIFT, PolyPhen-2, MutationTaster, PROVEAN, and AlphaMissense offer functional predictions for gene variants utilizing amino acid sequence information, sequence conservation, biophysical properties, or homolog alignment[25–30]. However, when given the same gene variants, these predictive tools may provide null values or contradicting results[31,32]. Indeed, the American College of Medical Genetics and Genomics and the Association for Molecular Pathology (ACMG-AMP), weights functional studies higher than in silico evidence for asserting pathogenic potential in gene variants for genes not previously established as causal for a particular disease[33–35]. We and others previously showed that functional testing of human gene variants is essential, as in silico approaches alone fail to reach the necessary accuracy for clinical translation[36–40]. While bioinformatics tools have greatly facilitated the functional interpretation of genetic variants[41–43], it is also important to note the essential role of functional validation of gene variants, especially for those genes where computational predictions tend to differ from experimental validation[44–50].

ESRP1 and its paralog *ESRP2* are epithelial splicing regulatory proteins that co-localize with *Irf6* and function in the embryonic epithelium to regulate craniofacial development and epithelial-mesenchymal transition

[1]Center for Craniofacial Innovation, Division of Plastic and Reconstructive Surgery, Department of Surgery, Children's Hospital of Philadelphia, Philadelphia, PA, USA. [2]Harvard Medical School, Boston, MA, USA. [3]Massachusetts General Hospital, Boston, MA, USA. [4]Department of Pathology and Laboratory Medicine, University of Pennsylvania Perelman School of Medicine, Philadelphia, PA, USA. [5]Shriners Hospital for Children, Tampa, FL, USA. [6]Department of Human Genetics, Emory University School of Medicine, Atlanta, GA, USA. [7]Center for Genomic Medicine, Department of Biomedical and Health Informatics, Children's Hospital of Philadelphia, Philadelphia, PA, USA. [8]Department of Medicine, University of Pennsylvania Perelman School of Medicine, Philadelphia, PA, USA. [9]Department of Surgery, University of Pennsylvania Perelman School of Medicine, Philadelphia, PA, USA. [10]These authors contributed equally: Caroline Caetano da Silva, Claudio Macias Trevino, Jason Mitchell. ✉e-mail: liaoce@chop.edu

during embryogenesis[22,51–53]. Global transcriptome analysis comparing mutant *irf6* and wildtype zebrafish revealed that the epithelial-specific splicing regulator *Esrp1* was differentially expressed[52]. We showed that *Esrp1* and *Esrp2* are colocalized in the periderm and oral epithelium and are required for the formation of the anterior neurocranium (ANC), a teleost embryonic structure developmentally analogous to the mammalian primary palate in the manner that it is formed from the convergence of frontonasal derived midline prominence and paired maxillary projections[54–57]. Targeted disruption of *Esrp1* in the mouse resulted in bilateral cleft lip and palate[21]. In the *esrp1/2* double homozygote zebrafish, cleft formed in the ANC and extended to the upper edge of the mouth opening, analogous to the cleft lip and/or palate (CL/P) phenotype observed in the *Esrp1/2* mutant mice[22,52]. In humans, biallelic *ESRP1* mutations were described to cause hearing loss[58], heterozygous *ESRP2* mutations were associated with CL/P[20] and both *ESRP1* and *ESRP2* splicing targets were related to cancer-associated processes[59]. Given the central role of *ESRP1* in periderm and embryonic epithelial development, there is likely selection against deleterious *ESRP1* alleles so that variants associated with hearing deficit are likely hypomorphic and homozygous or biallelic loss-of-function alleles are likely embryonic lethal and not observed clinically.

Here, we applied complementary in vivo and in vitro models to functionally interrogate human *ESRP1* and *ESRP2* gene variants. To increase the rigor of the functional test using another independent assay, we also examined Esrp-mediated alternative splicing in a murine *Esrp1/2* double knockout Py2T cell model. The Py2T cell line has been used effectively to study epithelial mesenchymal transition and we have previously generated and characterized Esrp1 and Esrp2 double knock-out Py2T lines[23,53]. Using these independent approaches, we functionally determined the pathogenicity of the 7 *ESRP1* and 12 *ESRP2* human gene variants from CL/P cohorts or reported in hearing loss. We previously showed that *Esrp1/2* regulated splicing of *Ctnnd1*[60]. Using RNAscope, we found that *Ctnnd1* transcripts co-localized with *Esrp1* and *Esrp2* in the mouse and zebrafish embryonic oral epithelium. The *esrp1/2* zebrafish model also presented a functional assay to test the function of Esrp-regulated genes such as *Ctnnd1*. In fact, exogenous expression of *ctnnd1* mRNA in zebrafish *esrp1/2* mutants partially rescued the cleft ANC, foreshortened pectoral fin and fused otolith phenotypes. Additionally, WGS of CL/P cohorts identified 13 new *CTNND1* gene variants, making this one of the most frequently associated genes in OFC. Taken together, these results demonstrate the critical requirement of *Esrp-Ctnnd1* operating in the embryonic epithelium to regulate palatogenesis.

Results

esrp1 and *esrp2* are required for morphogenesis of epithelial-derived tissues

We previously described the genetic requirement of *esrp1/2* in zebrafish epithelial development, disruption of which resulted in tethering of the upper mouth opening extending into a separation of the ANC, a phenotype morphologically analogous to CL/P of amniotes[52]. Given the expression of *esrp1/2* and in periderm and embryonic epithelial cells broadly, we examined other structures formed by epithelial origins. It was reported that *Esrp1* regulated the alternative splicing of *Arhgef11*, which was described to be important for proper otoliths development in zebrafish[61]. When the *esrp1/2* double mutants were examined at 4 dpf, we discovered that more than 90% of the mutant larvae exhibited at least one fused otolith (Fig. 1A, B).

Ventral cartilages that form with epithelial–mesenchymal interactions were also dysmorphic, where Meckel's cartilage appeared longer in the anteroposterior axis and narrower in the coronal axis. These morphologic differences can be captured by measuring the distance between Meckel's and ceratohyal cartilages which is extended in the *esrp1/2* mutants (Fig. 1C, D). We also detected partial penetrance of loss of ceratobranchial cartilages in 30% of the *esrp1/2* double mutant larvae at 7 dpf, and these larvae also exhibited loss of pharyngeal teeth (Fig. 1E).

Epithelial-mesenchymal interaction is also required for pectoral fin development. We observed that the *esrp1/2* double mutants exhibit foreshortened and curled pectoral fins, where the *sox10* labeled chondrocytes that populate the mesenchymal component and the *krt4* labeled epithelial populations are both decreased in cell number in the *esrp1*$^{-/-}$; *esrp2*$^{-/-}$ fins at 4 dpf (Fig. 1F). Whereas the wildtype fins extend and fan out as they develop to 4 dpf, the fins in the *esrp1*$^{-/-}$; *esrp2*$^{-/-}$ larvae curl proximally and are typically stuck to the torso through epithelial attachments.

In vitro and in vivo assays to functionally test *ESRP1* and *ESRP2* human gene variants

In a previous study we showed that *esrp1*$^{-/-}$; *esrp2*$^{+/-}$ intercross yielded Mendelian ratio of 25% *esrp1*$^{-/-}$; *esrp2*$^{-/-}$, and that injection of morpholino against *esrp2* in the *esrp1*$^{-/-}$ mutant embryos can consistently phenocopy the *esrp1*$^{-/-}$; *esrp2*$^{-/-}$ double mutant (Fig. 2A)[52]. This *esrp1*$^{-/-}$; *esrp2* MO model provides significant advantages over *esrp1*$^{+/-}$; *esrp2*$^{+/-}$ intercross, as the entire clutch of the *esrp1*$^{-/-}$ embryos injected with *esrp2* MO consistently exhibited the cleft ANC phenotype greatly facilitating detection of rescue of injected *ESRP1/2* mRNA to be tested.

We found that over-expression of wildtype zebrafish and human *ESRP1* and *ESRP2* mRNA rescued the cleft ANC phenotype in *esrp1*$^{-/-}$; *esrp2* MO embryos (Fig. 2B)[52]. Alcian blue staining of *esrp1*$^{-/-}$; *esrp2*$^{-/-}$ zebrafish at 4 dpf revealed a cleft ANC phenotype where a population of chondrocytes in the medial ANC is absent. A similar phenotype is observed when translation-blocking anti-*esrp2* morpholinos were injected into *esrp1*$^{-/-}$ embryos (Fig. 2A).

To functionally test human *ESRP1* or *ESRP2* gene variants, we introduced point mutations into zebrafish *esrp1* or *esrp2* coding sequences and subsequently co-inject 8 ng of anti-*esrp2* MO with either: (1) capped *esrp1* mRNA, (2) capped *esrp2* mRNA mutagenized with synonymous mutations at the MO binding site, or (3) either *esrp1* mRNA encoding for human *ESRP1* gene variants of unknown significance, or (MO-resistant) *esrp2* mRNA encoding for human *ESRP2* gene variants of unknown significance. We hypothesized that benign variants that preserve protein function would robustly rescue the cleft ANC phenotype like native *esrp1* or *esrp2* mRNA. Conversely, pathogenic human *ESRP1/2* gene variants with loss-of-function would fail to rescue the cleft ANC phenotype (Fig. 2B). Human *ESRP1* and *ESPR2* gene variants were cloned by site-directed mutagenesis, and synthesized mRNA was injected with *esrp2* MO into one-cell stage *esrp1*$^{-/-}$ embryos. The *esrp2* cDNA was engineered to prevent hybridization of the *esrp2* MO to the synthesized mRNA.

In order to gain additional functional assessment of the gene variants, we developed an independent in vitro assay using *Esrp1/2* mutant Py2T cells[62]. The murine Py2T epithelial cell line was developed where *Esrp1* and *Esrp2* were ablated using CRISPR-mediated gene editing. The *Esrp1/2*$^{-/-}$ Py2T cells exhibited splicing deficiencies in the *Esrp* target gene, *Arhgef11* (Fig. 2C)[62]. RT-PCR performed on wildtype Py2T cell cDNA using primers spanning splice junctions for *Arhgef11* demonstrated the presence of two major isoforms. The difference between these two isoforms is the presence or absence of exon 37, which is included in mesenchymal cells, but skipped in Py2T epithelial cells[23,63,64]. Py2T cells carrying *Esrp1* and *Esrp2* loss-of-function alleles preferentially expressed the longer mesenchymal isoform of *Arhgef11*.

We found that over-expression of *Esrp1* or *Esrp2* in the *Esrp*1/2 DKO Py2T cells efficiently rescued RNA-splicing to generate the epithelial isoform of *Arhgef11* transcript (Fig. 2C).

Identifying human *ESRP1* and *ESRP2* gene variants

Genome sequencing efforts have deposited numerous gene variants in publicly available repositories, including the Gabriella Miller Kids First (GMKF) Pediatric Research Program and ClinVar[65–67]. We filtered sequencing data from both repositories for patients with OFC or autosomal recessive deafness[20,58] and identified gene variants for either *ESRP1* or *ESRP2* to generate a list of 32 potentially disease-associated gene variants.

Because we are utilizing in vivo assay in zebrafish and in vitro assay in murine Py2T cells, we prioritized those human *ESRP1* and *ESRP2* gene

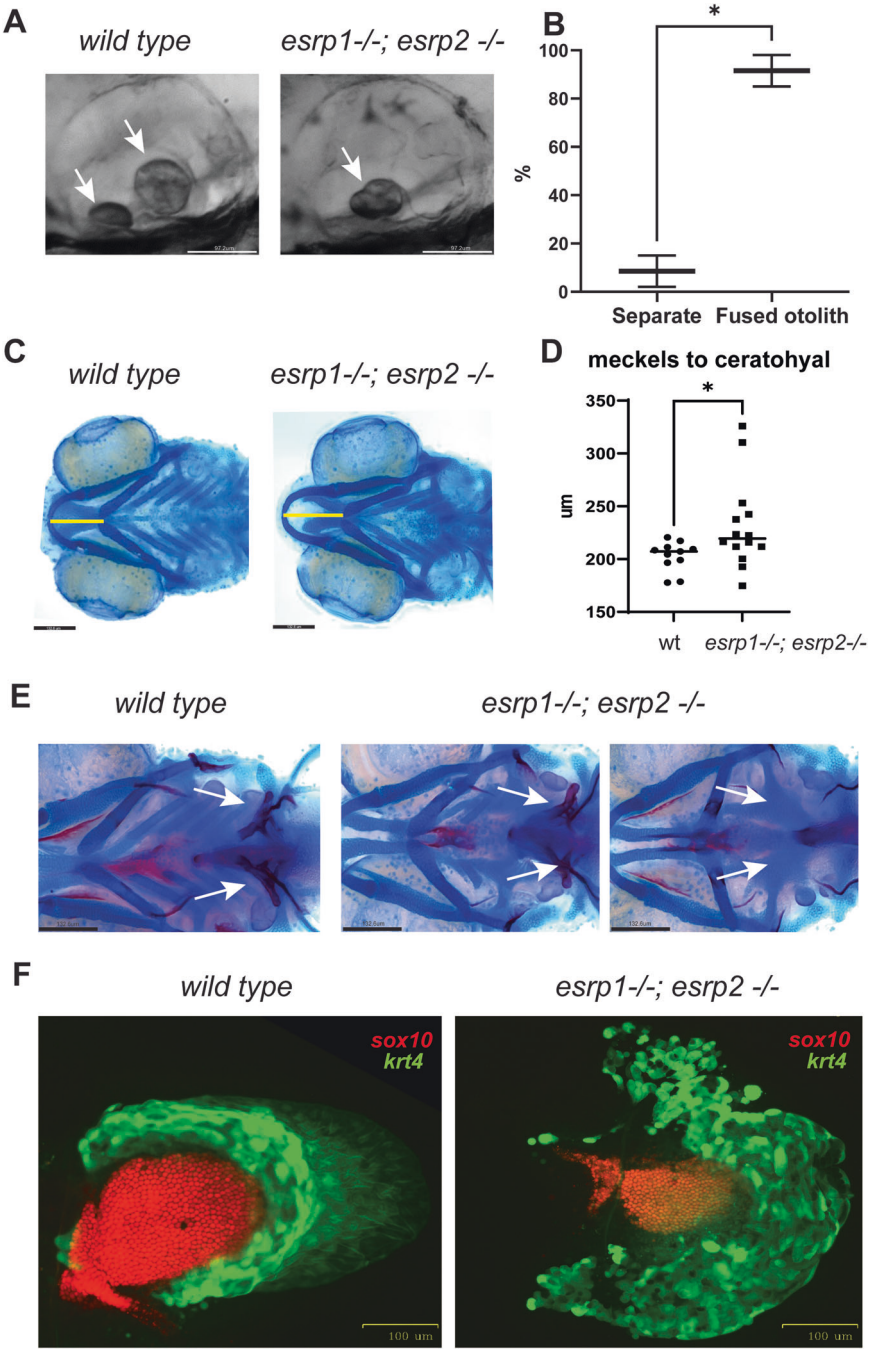

Fig. 1 | *esrp1* and *esrp2* are required for morphogenesis of epithelial-derived tissue: otoliths, pharyngeal teeth and pectoral fins. A zebrafish otoliths indicated by white arrows at 72 hpf. **B** Quantification and t-test of zebrafish otoliths from genotyped mutants characterized as separate or fused otoliths. t-test, $n = 75$. **C** Alcian blue representation of a 6 dpf zebrafish wildtype and esrp1$^{-/-}$ esrp2$^{-/-}$ double mutant showing cartilage stain, yellow line shows the measurement of the distance between the midline of Meckel's and ceratohyal cartilages. **D** quantification and t-test analysis of this measurement in wildtype ($n = 11$) and *esrp1*$^{-/-}$; *esrp2* $^{-/-}$ mutants ($n = 14$). **E** Alcian blue and Alizarin red staining of larvae at 7 dpf ventral view, the pharyngeal teeth are present in wildtype (white arrows). In contrast, the *esrp1*$^{-/-}$; *esrp2*$^{-/-}$ all exhibit decreased number of teeth, and occasionally some double mutants lack all ceratobranchial cartilages and the pharyngeal teeth are absent. **F** wildtype and esrp1$^{-/-}$ esrp2$^{-/-}$ mutant pectoral fins labeled with *sox10* mCherry (red) and *krt4* gfp (green).

variants residing in cross-vertebrate conserved residues. For ESRP1, the overall amino acid sequence identity was 97% and 64.68% between humans and mice, or humans and zebrafish, respectively. However, when focusing on the RNA-recognition motif (RRM) domains of ESRP1, the similarity of the sequences between humans and mice and humans and zebrafish increased to 98.82% and 94.12% for RRM1, 99.08% and 79.82% for RRM2, and 95.06% and 77.78% for RRM3. Similarly, for ESRP2, the overall amino acid sequence similarity was 98.67% between humans and mice and 85.33% between humans and zebrafish. The domain-specific amino acid sequence similarities were 98.67% and 85.33% for RRM1, 98.13% and 81.31% for RRM2, and 96.3% and 77.78% for RRM3 between humans and mice, and humans and zebrafish, respectively. Altogether, we identified 19 out of the 32 gene variants in residues fully conserved between human, mouse, and zebrafish. Gene variants were evenly spread throughout both proteins and included two variants in the RRM1 domain of *ESRP1* and two variants each in the RRM1, RRM2, and RRM3 domains of *ESRP2* (Fig. 1 Supplementary Material).

We found that the in silico predictions from SIFT and Polyphen-2 followed one of four patterns: (1) concordant predictions from both tools annotating the variant as benign, (2) concordant predictions from both tools annotating the variant as damaging, (3) discordant predictions from both tools, (4) tools unable to predict the effect of the variant on protein function (Table 1). Altogether, two variants from *ESRP1* (E194A and N643S) and two variants from *ESRP2* (C372S and T475T) were predicted by both SIFT and PolyPhen-2 to have a benign effect on protein function. One variant from *ESRP1* (Q90R) and four from *ESRP2* (R250Q, R315H, R353Q, and R667C) were predicted by both to have a deleterious effect on protein function. SIFT and PolyPhen-2 do not offer predictions for three truncation variants (*ESRP1* D222fs, *ESRP2* R520*, and *ESRP2* E547del). However, the remaining three *ESRP1* variants (L259V, K287R and Y605F) and four

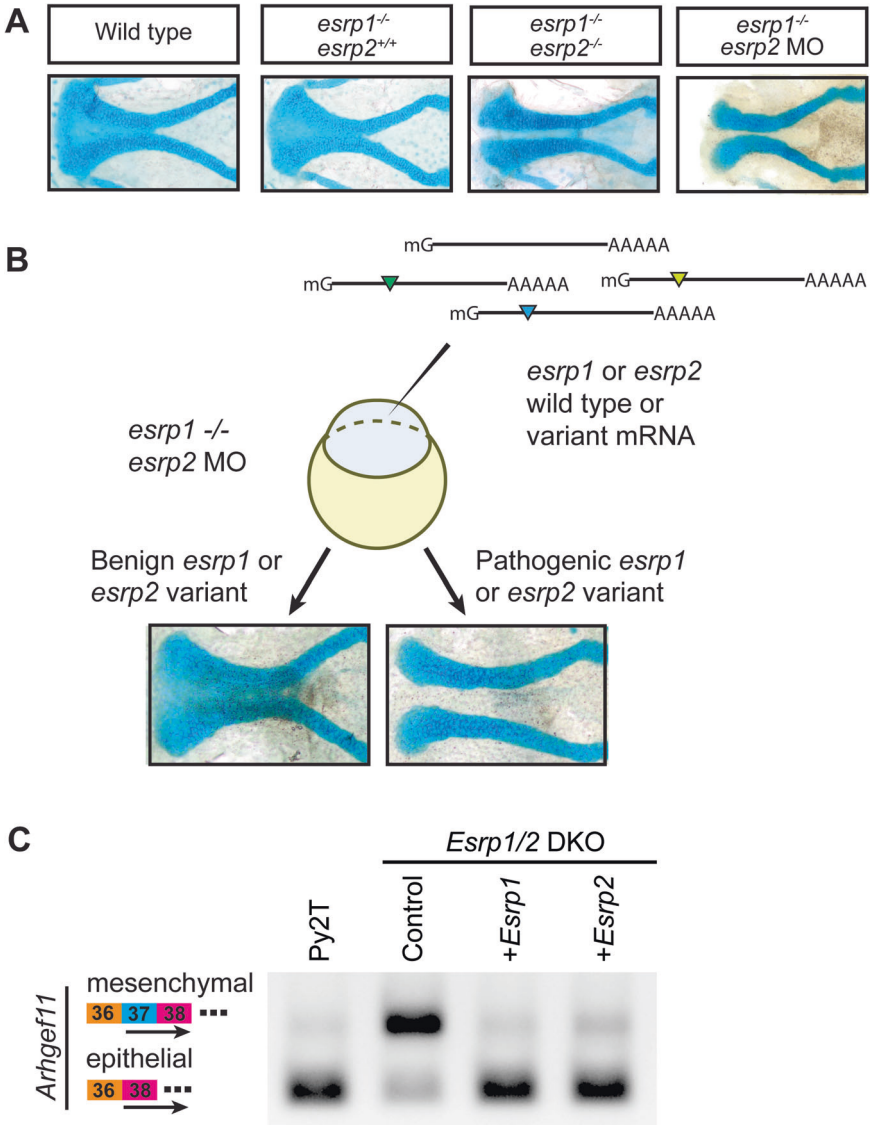

Fig. 2 | Complementary in vivo and in vitro functional assays to test human *ESRP1* and *ESRP2* gene variants. A Microdissected ANC of Alcian-blue stained embryos at 4 dpf for wildtype, *esrp1*$^{-/-}$; *esrp2*$^{+/+}$, *esrp1*$^{-/-}$; *esrp2*$^{-/-}$, and *esrp1*$^{-/-}$; *esrp2 MO* embryos. **B** Schematic for the *esrp* morphant variant assay in zebrafish. Variants that robustly rescued the cleft ANC phenotype were scored as benign, while variants that failed to rescue the cleft ANC phenotype were scored as pathogenic. **C** RT-PCR was performed using primers spanning exons 36–38 of *Arhgef11* on cDNA isolated from wildtype mouse Py2T cells, *Esrp1/2* double-knockout Py2T cells, or *Esrp1/2* double-knockout PyY2T cells electroporated with plasmids encoding for either *Esrp1* or *Esrp2* genes. Arrow markers point to the epithelial (short) isoform and mesenchymal (long) isoform retaining exon 37.

ESRP2 variants (L92Q, S508L, R437H, and L665W) had discordant predictions between both algorithms. Thus, in silico predictions were not adequate to annotate roughly half of the selected gene variants and required an alternate approach to predict their effects on protein function.

Functional testing of *ESRP1* and *ESRP2* variants in zebrafish and murine Py2T cell assays

The selected 19 *ESRP1* and *ESRP2* gene variants were experimentally tested in zebrafish and Py2T cell assays. SDM was carried out in *ESRP1* and *ESRP2* cDNA sequences and cloned into the pCS2 + 8 vector backbone to generate capped mRNA for microinjection into zebrafish embryos. The zebrafish assay was optimized by microinjection of *esrp2* translation-blocking morpholinos into *esrp1*$^{-/-}$ intercross, because the *esrp2*$^{-/-}$ females are infertile[22]. However, since the *esrp2* MO would also neutralize exogenous injected *ESRP2* mRNA upon co-injection into zebrafish embryos, synonymous mutations were introduced in the translational start site of the pCS2 + 8-*Esrp2* plasmid, to generate *esrp2* MO-resistant *ESRP2* mRNA transcripts. Co-injection of 8 ng of *esrp2* MO with 200 pg of either *ESRP1* mRNA or MO-resistant *ESRP2* mRNA fully rescued the ANC phenotype in over 75% of 19 injected clutches at 4 dpf (Fig. 3A).

To test for the ability of human *ESRP1/2* gene variants to rescue the cleft ANC phenotype in zebrafish, each of the 19 *ESRP1* or *ESRP2* gene variants was co-injected with *esrp2*-MO into *esrp1*$^{-/-}$ zebrafish embryos. At 4 dpf, the injected fish were fixed, stained with Alcian Blue, and analyzed. We found that for *ESRP1*, all six missense variants rescued the ANC phenotype. Only one variant, a frameshift mutation at the 222 aspartate residue (D222fs), had a large proportion of cleft ANC in the injected clutch compared to embryos injected with wildtype *esrp1* mRNA, and was scored as a pathogenic variant (Fig. 3B). For *ESRP2*, 10 out of 12 tested gene variants rescued the ANC phenotype, in a ratio like the *esrp2* mRNA control and were scored as benign variants. The silent mutation T475T, served as an internal negative control and also scored as benign. The remaining two *ESRP2* gene variants (R315H and R520*) failed to rescue the ANC phenotype and were scored as pathogenic (Fig. 3C).

To independently assess the gene variant functional testing results obtained from the zebrafish model, we tested 3 *ESRP1* and 8 *ESRP2* human gene variants using the mouse Py2T cell assay, with epithelial-specific RNA splicing of *Arhget11* as the readout (Fig. 3D, E). We aimed to obtain an additional functional assessment for those gene variants testing results that contradicted in silico prediction. We performed site-directed mutagenesis (SDM) to introduce the 11 gene variants, that were electroporated into *Esrp1/2* DKO PY2T cells and performed the RT-PCR assay 24 h post-electroporation. We found that for *ESRP1*, gene variant L259V restored *Arhgef11* restriction to the epithelial isoform was scored as damaging for Polyphen-2 and Alpha missense and benign for SIFT (Fig. 3, Table 1). The frameshift variant, D222fs, that was pathogenic in the in vivo assay was also

Table 1 | *ESRP1* and *ESRP2* variants classification

ESRP1	Protein Domain	PolyPhen-2	SIFT	Alpha Missense	Zf in vivo assay	Py2T in vitro assay	Interpretation
Q90R		Damaging	Damaging, LC	Benign	Rescue	n/a	Benign
E194A		Benign	Benign	Benign	Rescue	n/a	Benign
D222fs		n/a	n/a	n/a	Mutant	Deficient	Damaging
L259V	RRM1	Damaging	Benign	Pathogenic	Rescue	Restored	Benign
K287R	RRM1	Damaging	Benign	Benign	Rescue	n/a	Benign
Y605F		Benign	Damaging, LC	Benign	Rescue	n/a	Benign
N643S		Benign	Benign	Benign	Rescue	Restored	Benign

ESRP2	Protein Domain	PolyPhen-2	SIFT	Alpha Missense	Zf in vivo assay	Py2T in vitro assay	Interpretation
L92Q		Benign	Damaging, LC	Likely pathogenic	Rescue	n/a	Benign
R250Q		Damaging	Damaging	Likely pathogenic	Rescue	Restored	Benign
R315H	RRM1	Damaging	Damaging	Likely pathogenic	Mutant	Deficient	Damaging
R353Q	RRM1	Damaging	Damaging	Likely pathogenic	Rescue	Restored	Benign
C372S	RRM2	Benign	Benign	Ambiguous	Rescue	n/a	Benign
R437H	RRM2	Damaging	Benign	Ambiguous	Rescue	n/a	Benign
T475T	RRM3	Benign	Benign	n/a	Rescue	Restored	Benign
S508L	RRM3	Damaging	Benign	Likely pathogenic	Rescue	Restored	Benign
R520STOP	RRM3	n/a	n/a	n/a	Mutant	Deficient	Damaging
E547del	RRM3	n/a	n/a	n/a	Rescue	n/a	Benign
L665W		Benign	Damaging, LC	Likely benign	Rescue	n/a	Benign
R667C		Damaging	Damaging, LC	Ambiguous	Rescue	Restored	Benign

pathogenic in this assay as it was unable to restore the epithelial isoform (Fig. 3D, Table 1). Interestingly, the *ESRP1* gene variant N643S partially restored some of the splicing function of *Esrp1*, where both epithelial and mesenchymal *Arhgef11* isoforms were detected in a 1:1 ratio (Fig. 3D). However, the same variant, N643S, in zebrafish rescued the phenotype. Statistical analysis for the Py2T rescue assay, can be found at Supplementary Fig. 2. These results suggest that *ESRP1* N643S variant may be hypomorphic, or that *Arhgef11* is just one readout of *Esrp1* mRNA splicing activity. Because *Esrp1* shows position-dependent repression of exon splicing of *Arhgef11*, it is possible that some domains or regions may be required, or not, for some specific functions. It is possible that some splicing events may be differentially affected by mutations and there are other suggested functions of *Esrp1* in mRNA stabilization or post-transcriptional regulation that are accounted for in the zebrafish rescue assay[60].

For *ESRP2*, variants R250Q, R353Q and R667C rescued the molecular splicing of *Arhgef11* in the Py2T assay, (Fig. 3E, Table 1). However, *ESRP2* gene variants R315H, S508L, and R520* failed to rescue deficient *Arhgef11* splicing in the Py2T assay and were scored as pathogenic, corroborating the pathogenic scoring from the zebrafish ANC rescue assay (Fig. 3E, Table 1).

Overall, we found that the in vivo zebrafish ANC rescue assay and the in vitro Py2T splicing assays were largely concordant to determine pathogenicity of the *ESRP1* and *ESRP2* gene variants tested. PolyPhen-2 correctly predicted the effect of 8/18 (44.4%) tested gene variants, while SIFT correctly predicted the effect of 7/18 (38.8%) gene variants. When the predictions of both algorithms were concordant, they correctly predicted the consequence of five out of seven (71.4%) gene variants on protein function (Table 1). The performance of concordant predictions was better for annotating benign variants where the algorithms correctly identified all four concordant benign variants with benign effects in both of our assays. Strikingly, the computational agreement incorrectly annotated two of four (50%) gene variants as pathogenic that had benign effects in both rescue assays. Ultimately, the algorithmic predictions were unable to determine half of the identified gene variants and greatly overestimated the prevalence of pathogenic variants (Table 1).

AlphaMissense over-interpreted pathogenic variants

Recently a new gene variant analysis tool AlphaMissense was released and purported to improve variant calling accuracy by leveraging protein structure information predicted by machine learning algorithm AlphaFold[68]. Using AlphaMissense to analyze the six *ESRP1* and nine *ESRP2* missense variants we had functionally tested, we observed that AlphaMissense classified five variants as benign for *ESRP1* (Q90R, E194A, K287R, Y605F, N643S) consistent with the functional tests, but called L259V as pathogenic when both the in vivo and in vitro functional tests demonstrated protein function (Fig. 4).

For *ESRP2*, AlphaMissense and the experimental validation were only concordant on two variants out of nine, calling R315H as pathogenic and L665W as benign (Fig. 4). AlphaMissense called six variants as pathogenic when they were shown to be functionally benign in both in vitro and in vivo functional tests. Therefore, our results showed that AlphaMissense may over-interpret variants as pathogenic for some genes.

Alternative splicing to generate epithelial isoform of Ctnnd1 requires Esrp1/2 function

We and others demonstrated that Esrp1 and Esrp2 regulate the alternative splicing of Ctnnd1, generating isoforms that differ between epithelial and mesenchymal cell types[20,60,62,69], making *Ctnnd1* an interesting *Esrp1/2* target that has also been implicated in CL/P[70].

CTNND1 (p120-catenin) has been associated with Blepharocheilodontic (BCD) syndrome and non-syndromic human CL/P[19,20,71]. Like other catenins, *Ctnnd1* has dual roles: it functions as part of the adherens junction cellular scaffolding to stabilize cell adhesion molecules, as well as a transcriptional regulator[19,72–76]. Furthermore, functional differences between epithelial and mesenchymal forms of *Ctnnd1* have been

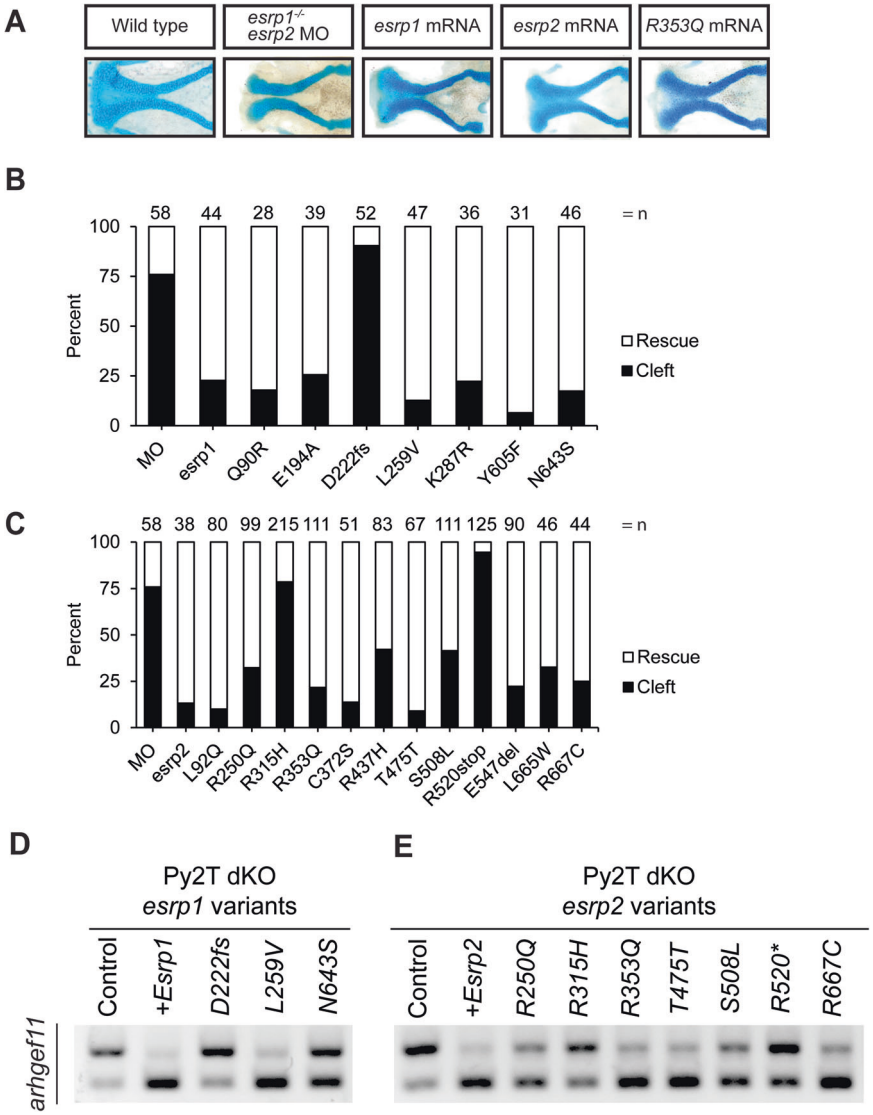

Fig. 3 | Functional testing of human ESRP1 and ESRP2 gene variants. A Representative images of the ANC from Alcian-blue stained larvae at 4 dpf after injection with *esrp2* MO and 200 pg of: *esrp1* mRNA, *esrp2* R353Q mRNA. ANC was scored as a rescued ANC or cleft ANC (**B**) *ESRP1* and (**C**) *ESRP2* gene variant rescue assay results for embryos injected with *esrp2* MO and 200 pg of *esrp1* variant mRNA. Results presented as percentage of rescue vs. cleft as different numbers of embryos survived and were analyzed, indicated as n above each bar. **D** *ESRP1* and (**E**) *ESRP2* gene variant rescue assay by detecting alternative splicing of Arhgef11 in murine Py2T wildtype and *Esrp1*$^{-/-}$; *Esrp2*$^{-/-}$ double knockout cells.

described[77–79]. Four major isoforms for *Ctnnd1* have been characterized in humans. The full-length isoform, isoform 1, has a translational start site at the first methionine in the sequence (1 Met), while isoforms 2, 3, and 4 undergo splicing events that cause a 5′ truncation of the transcript and change the translational start site to methionines 55, 102, and 324, respectively. Isoform 1 of *CTNND1* is predominantly expressed in the mesenchyme, while the shorter isoform 3 is restricted to the epithelium. The remaining isoforms, 2 and 4, are less abundant and have not been thoroughly characterized[71].

When we aligned the amino acid sequences between human, mouse, and zebrafish *Ctnnd1* homologs, we found that methionine in positions 1 and 102 is conserved in all three species. Methionine 55 is part of a 14 aa stretch absent in zebrafish (Fig. 5A). Given that transcripts for the long (mesenchymal) isoform shift to the shorter (epithelial) isoform by splicing out a 5′ exon(s) and moving down to a conserved methionine, splicing patterns are well-conserved across human, mouse, and zebrafish. Cox et al reported that *ESRP2* and a short form of the full-length *CTNND1* protein, identified by an antibody to the C-terminus, are colocalized in the periderm of human embryos[20]. Meanwhile, RNA splicing of *Ctnnd1* transcripts is deficient in the embryonic epithelium of *Esrp1*$^{-/-}$ mice[53].

We confirmed that long and shorter *Ctnnd1* isoforms were found in the mouse Py2T cells by performing RT-PCR using primers spanning exon 2, which is partially skipped in the shorter isoform for *Ctnnd1*. In the *Esrp1/2*$^{-/-}$ Py2T cell line, the splicing pattern of *Ctnnd1* shifts and is biased towards the longer mesenchymal isoform, confirming previous observations[60].

To localize *Ctnnd1* and *Esrp1/2* gene expression in wildtype mouse and zebrafish, we carried out RNAscope and BaseScope on wildtype and mutant mouse and zebrafish sections (Fig. 5B, C). The *Ctnnd1* probe used identifies shared C-terminal exons shared in all *Ctnnd1* isoforms. Only *Esrp1* probe was used here as we and others have previously shown that *Esrp1* and *Esrp2* gene expression are co-localized in mouse and zebrafish[21,22,52,62]. In zebrafish, *ctnnd1* and *esrp1* RNAscope signals are co-localized robustly throughout the oral epithelium with sparse signals in the mesenchyme.

To assess the tissue specific distribution of the longer mesenchymal isoforms of *Ctnnd1* vs. shorter epithelial isoform, BaseScope probes were used to detect the two *Ctnnd1* isoforms from wildtype and *Esrp1*$^{-/-}$; *Esrp2*$^{-/-}$ mutant mouse at E15. Similar to RNAScope result in zebrafish (Fig. 5B), the murine *Ctnnd1* BaseScope signals for both mesenchymal and epithelial isoforms were robust in the oral epithelium and sparsely scattered in the mesenchyme (Fig. 5D, G). When signal is differentiated by isoform, the longer *Ctnnd1* mesenchymal isoform was uniformly distributed throughout the epithelium and mesenchyme (Fig. 5E, H). However, the shorter *Ctnnd1* epithelial isoform was restricted to the epithelial cells and excluded from the muscle (Fig. 5F, I). In the wildtype, BaseScope signals of the longer *Ctnnd1* mesenchymal isoform appeared equally distributed in the mesenchyme and epithelium, and the signals of

Fig. 4 | AlphaMissense pathogenicity predictions for ESRP1 and ESRP2 missense variants. *ESRP1* and *ESRP2* gene variants from OFC cases in the GMFK Children's dataset and ClinVar variants associated with cleft lip and/or palate or autosomal recessive deafness were identified. Six ESRP1 and nine ESRP2 (**A**), (**D**) missense variants were analyzed using the AlphaMissense (AM) model. The tables (**C**), (**F**) show the AM-predicted pathogenicity compared to our functional test results and the AM mutation score, which is also graphed. On the left, the *ESRP1* and *ESRP2* AlphaFold structures (**B**), (**E**), with labeled missense mutations, color-coded with the functional results.

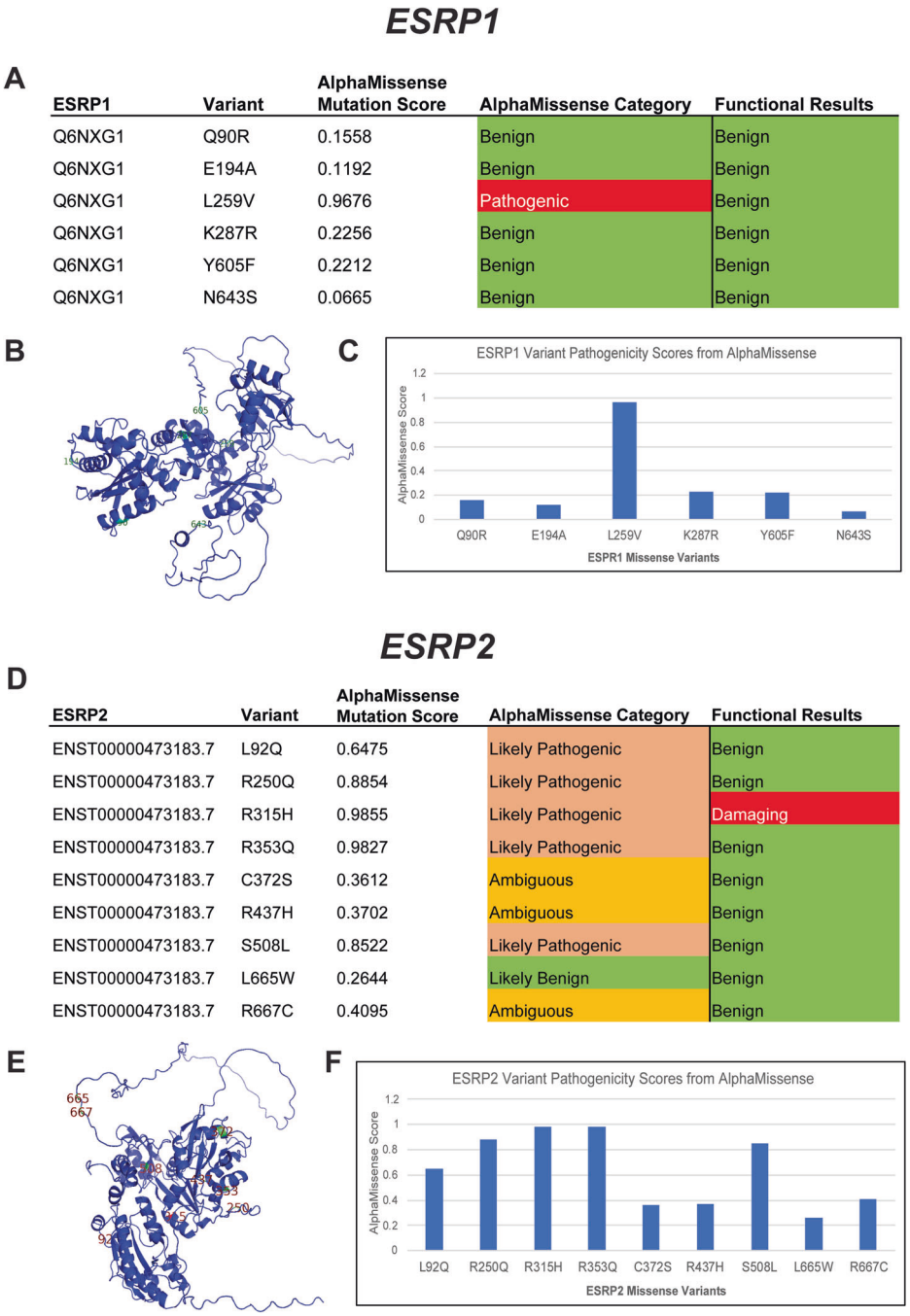

the shorter isoform was epithelial restricted. In the *Esrp1*$^{-/-}$; *Esrp2*$^{-/-}$ mutant mouse, *Ctnnd1* transcript level was significantly reduced and predominantly the longer *Ctnnd1* mesenchymal isoform was detected, in both the mesenchyme and epithelium. The shorter *Ctnnd1* epithelial isoform was sparsely detected via BaseScope in the *Esrp1*$^{-/-}$; *Esrp2*$^{-/-}$ mutant, consistent with the finding where shorter isoform was significantly reduced in the *Esrp1*$^{-/-}$; *Esrp2*$^{-/-}$ Py2T cells by qPCR. These results corroborate that Esrp1/2 is required for RNA splicing of *Ctnnd1*, generating the shorter isoform specifically in the epithelium but not the mesenchyme.

CTNND1 gene variants from OFC cohorts

Twenty-four *CTNND1* gene variants have been reported and a growing number of new variants have been found in ongoing WGS studies of OFC cohorts[19,26]. In a recent analysis of 759 OFC trios, we identified 15 variants in *CTNND1* with allele frequencies less than 0.1% in gnomAD (Fig. 3, Supplementary Material). Two variants were de novo and one was inherited from an affected parent. Pathogenic variants in *CTNND1* accounted for 0.8% of the cohort. Only 10% of the cohort had a pathogenic variant in 500 genes implicated in OFC that we analyzed, making *CTNND1* the mostly frequently mutated variant in this cohort[70]. In the gene-based burden test, rare variants were nominally over-transmitted to affected children ($p = 0.06$); de novo variants are enriched in *CTNND1* ($p = 0.005$ for loss-of-function de novo variants; 0.001 for protein-altering de novo variants). Nearly all the missense variants were classified as variants of unknown significance, indicating that functional testing is critical. In fact, we estimate that *CTNND1* mutations account for at least 1.5% of CL/P cases. By comparison, *IRF6* mutations are estimated to be the most common cause of CL/P, accounting for 2% of cases. Taken together, *CTNND1* stands to be as important as *IRF6* in contributing to the genetic risk of syndromic and non-syndromic CL/P.

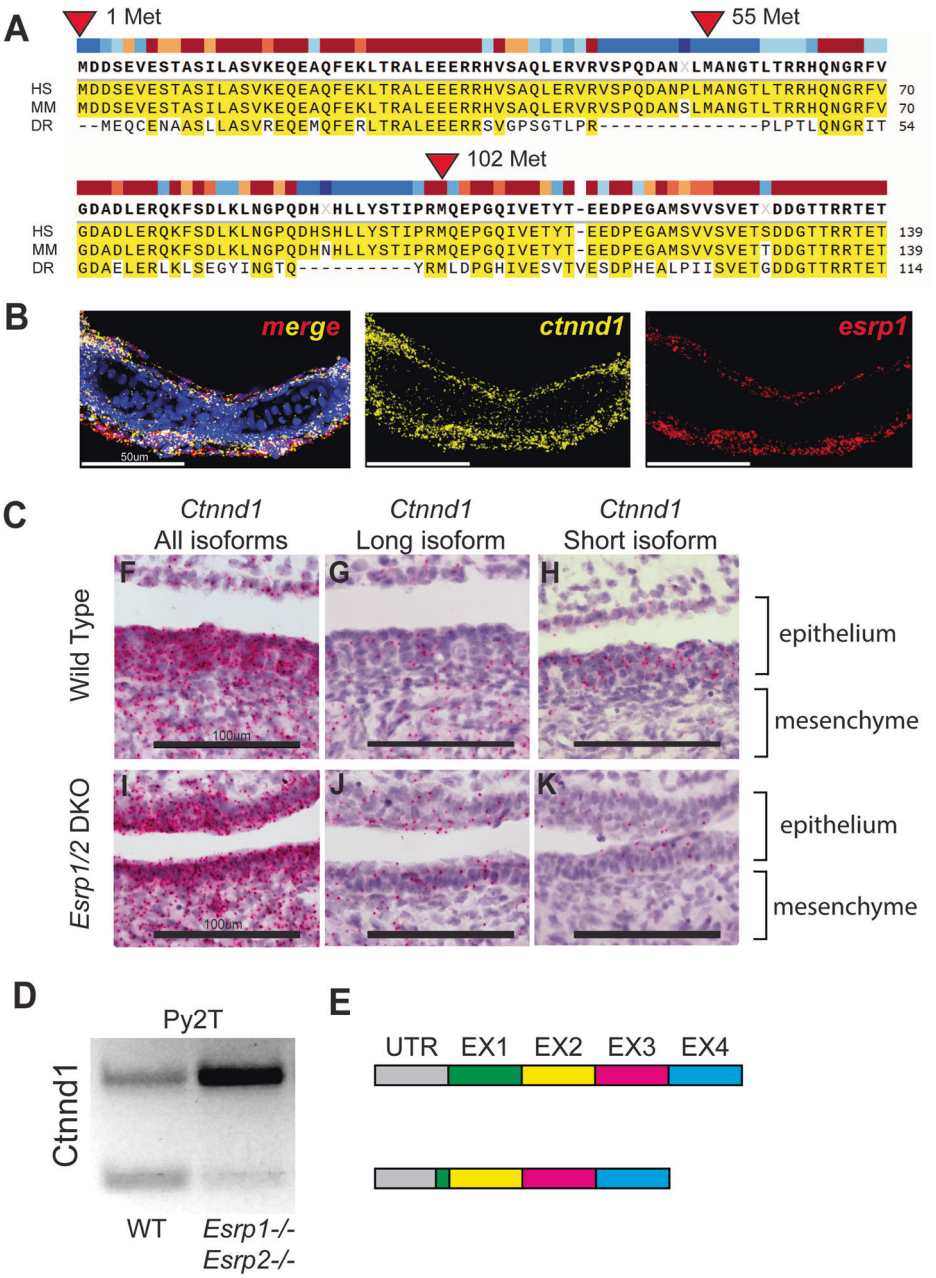

Fig. 5 | Alternative splicing of *Ctnnd1* is regulated by Esrp1/2. A Amino acid sequence alignment of the first 140 residues of CTNND1 protein across human, mouse, and zebrafish. Translation for isoform 1 of CTNND1 begins at methionine 1, while isoform 3 encodes a truncated form that starts translation at methionine 102. Methionine residues at positions 55 and 324 are not conserved across all three species. **B** Detection of *esrp1* and *ctnnd1* gene expression in zebrafish at 4 dpf, demonstrates shared localization of transcripts in the embryonic epithelium. This coronal section includes the ventral Meckel's cartilage. **C** Detection of murine *Ctnnd1* mRNA using isoform-specific base-scope probes in the oral epithelium and tongue mesenchyme. The wildtype sections show that the *Ctnnd1* long isoform is present in both epithelial and mesenchymal cells. The *Ctnnd1* short isoform is present preferentially in epithelial cells and not in the mesenchymal cells. In the *Esrp1/2* DKO mouse, the mesenchymal *Ctnnd1* long isoform is detected in epithelial and mesenchymal cells, with loss of the *Ctnnd1* short isoform. **D** RT-PCR of the *Ctnnd1* long and short isoforms from Py2T cells. **E** Diagrammatic representation of the ESRP-regulated *CTNND1* alternative splicing to generate the shorter epithelial isoform.

Ctnnd1 over-expression rescue *esrp1*$^{-/-}$; *esrp2*$^{-/-}$ cleft ANC, curled fin and fused otolith phenotypes

To functionally assess the relationship between *Esrp* and *Ctnnd1*, we injected the zebrafish *ctnnd1* isoform-201 (ENSDART00000106048.4) mRNA into *esrp1*$^{-/-}$; *esrp2*$^{+/-}$ offspring at the 1-cell stage. Mutants and control embryos were analyzed at 4 dpf, assessing the ANC, the pectoral fin, and otoliths phenotypes, followed by genotyping (Fig. 6A).

Control *gfp* mRNA injected *esrp1*$^{-/-}$; *esrp2*$^{-/-}$ larvae, exhibited cleft ANC, the pectoral fins were hypoplastic and stuck to the thorax, and fused otoliths, the mutant phenotypes were fully penetrant and reliably scored (Fig. 6B–E). In the *ctnnd1* mRNA injected *esrp1*$^{-/-}$; *esrp2*$^{-/-}$ larvae, 22% ($n = 20$ of 90, $p < 0.01$) demonstrated a full or partial rescue of the ANC (Fig. 6B–E). Correspondingly, the injected *esrp1*$^{-/-}$; *esrp2*$^{-/-}$ larvae exhibited significant rescue of the abrogated fin phenotype, with 21% ($n = 19$ of 90, $p < 0.01$) exhibiting extension of the pectoral fin and angling away from the thorax. The fused otolith phenotype was scored as either separate or fused, and demonstrated 26% ($n = 26$ of 90, $p < 0.01$) rescue (Fig. 6A). The morphogenesis of the ANC, pectoral fin and the otoliths all reflect different aspects of embryonic epithelium development and interaction with the associated mesenchyme of the *esrp1*$^{-/-}$; *esrp2*$^{-/-}$ embryos. The *ctnnd1* mRNA over-expression rescuing the epithelial defects in the *esrp1*$^{-/-}$; *esrp2*$^{-/-}$ suggests that a key function of *esrp1/2* in epithelial biology is to regulate *ctnnd1* function.

Discussion

Several independent lines of evidence corroborate that the *ESRP1* and *ESRP2* genes are important OFC loci in humans. *ESRP1* was proposed to be the most likely candidate CL/P risk gene in the 8q22.1 locus[80,81]. Ectopic expression of p63 converted human fibroblasts to keratinocyte-like cells and *ESRP1* was transcriptionally induced together with activation of an epithelial enhancer within a topologically associated domains containing a non-syndromic CL/P risk locus[82]. This is consistent with the biological observation and *p63*, *Irf6* and *Esrp1/2* co-localize in the embryonic epithelium, and that mutations of these three genes result in OFC phenotypes.

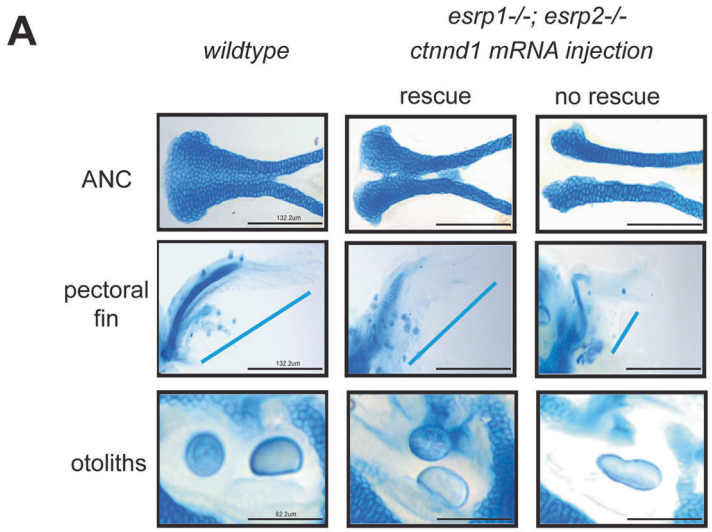

B

esrp1-/-; esrp2	control GFP mRNA			*ctnnd1* mRNA		
	+/+	+/-	-/-	+/+	+/-	-/-
Total	38	70	43	65	146	90
wildtype ANC	38	62	0	61	134	2
partial cleft ANC	0	3	4	3	6	18
cleft ANC	0	5	39	1	6	70
wildtype fins	36	62	2	57	136	19
curled fins	2	8	41	8	10	71
Normal otoliths	38	69	1	65	138	26
Fused otoliths	0	1	42	0	8	64

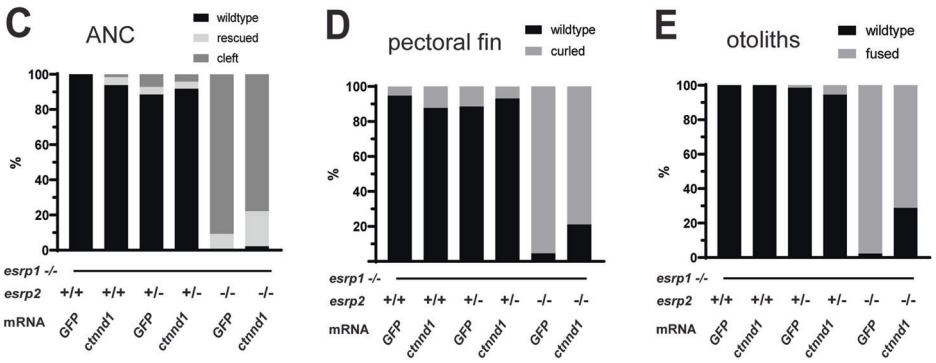

Fig. 6 | Over-expression of *ctnnd1* rescues esrp1$^{-/-}$, esrp2$^{-/-}$ epithelial phenotypes. A Image representing how wildtype, intermediate and cleft ANC, pectoral fins and otoliths were sorted. **B** Representative table with the number of total fish injected and rescued by the *ctnnd1* mRNA injection with GFP mRNA injection as control. Scoring of ANC phenotype (%) (**C**), fin phenotype (%) (**D**) and the otolith phenotype (%) (**E**) in the injected *esrp1*$^{-/-}$; *esrp2*$^{+/-}$ inter-cross larvae confirmed by genotyping, showing 20–22% rescue of ANC, fin and otolith phenotypes in the *esrp1*−/−; *esrp2*$^{-/-}$ double homozygous larvae.

Further, a whole exome sequencing study of non-syndromic CL/P in multi-affected families identified pathogenic variants in *ESRP2* with an autosomal dominant inheritance pattern[20].

Several studies showed in mouse and zebrafish models that *Esrp1* and *Esrp2* are important in craniofacial development. We showed that *Esrp1* and *Esrp2* are co-localized with *Irf6* in the embryonic oral epithelium, and when *Ersp1/2* are disrupted, cleft of the lip and palate formed, validating that mouse and zebrafish are robust animal models of human OFC[21,52,53].

There is growing recognition that RNA-binding proteins that regulate alternative splicing play vital roles in craniofacial morphogenesis. Clinically, spliceosomopathies are often associated with syndromic craniofacial abnormalities due to disruption of splicing factors such as *PUF60*, *ETUD2*, *SF3B4*, *RBM10*, and *ESRP2*[83]. Animal models defective in RNA splicing that exhibit craniofacial phenotypes include: *Esrp1/2, Rbfox2*, *Srsf3*, and *Sf3b2*[21,22,52,84,85]. The ESRP proteins are uniquely expressed in epithelial structures and direct post-transcriptional modifications that distinguish protein isoforms between epithelium and mesenchyme. We applied complementary phenotypic and molecular assays to interrogate the functional consequence of identified *ESRP1/2* gene variants in cohorts of autosomal recessive deafness and CL/P.

As the magnitude of available WGS data increases, the need for assigning clinically actionable information continues to grow. The sequence variant interpretation working group from ACMG-AMP frequently reconvenes to update, revise, and refine the ACMG criteria to provide the clearest guidance possible[33,34]. Most recently, the working group provided further guidance regarding functional assays and experimental model systems. Among these, they highlighted the need to ascertain the gene variants' physiologic context and molecular consequence. Here, we applied complementary phenotypic assays in the zebrafish ANC rescue, in addition to the Py2T splicing assay, to assess the physiologic and molecular consequences of *ESRP1/2* gene variants observed in clinical cohorts. These functional tests identified seven pathogenic variants out of 18 *ESRP1/2* variants examined. Moreover, these functional readouts of orthologous systems across species attest to the strongly conserved nature of epithelial splicing by the *ESRPs* in craniofacial morphogenesis. These results highlight the need for experimental models to enhance the validity of in silico predictions of protein function. We found that while the SIFT and PolyPhen-2

algorithms have a positive predictive value when they align in predicting benign variants, they tend to overestimate the prevalence of pathogenic variants.

While AlphaMissense provided slightly better predictions for *ESRP1* than SIFT and PolyPhen-2, in the case of *ESRP2*, AlphaMissense over-interpreted benign variants as pathogenic. A similar high false positive rate was seen in a different disease, cystic fibrosis transmembrane conductance regulator[86], and for epithelial master regulator *IRF6*[87]. This work highlights that protein structure and machine learning approaches today are still insufficient to accurately predict pathogenicity, where functional tests are indispensable to validate the pathogenicity of variants.

These functional assays revealed novel insights into *ESRP1/2* protein function and downstream targets spliced by the *ESRP*s. We found that the gene variants with the largest effect size for the zebrafish ANC rescue assay lie in RRM1 and RRM3 of *ESRP2*. Variants R250Q and R353Q were predicted by PolyPhen-2, SIFT, and AlphaMissense to be damaging or likely pathogenic, but in both independent functional tests corroborated to be benign variants. In contrast, R315H was functionally tested by both assays to be a deleterious variant, consistent with prior work demonstrating R315 to impact RNA binding based on protein structure analysis[88]. Furthermore, we provide molecular evidence that *Esrp* transcripts rescue molecular splicing patterns of putative *Esrp*-target genes *Arhgef11* and *Ctnnd1*. Moreover, gene variants with pathogenic potential do not restore splicing patterns of *Arhgef11*, providing evidence that the gene variants impair *Esrp* function and likely contribute to disease pathogenicity. These functional assays provide key data to satisfy the ACMG-AMP standards, where molecular assays are used to contribute to our understanding of mechanisms for disease.

Mutations in *CTNND1* and *CDH1* (E-cadherin) are the known cause of BCD, which includes abnormal eyelids, upper lip, palate, and teeth development[20,71,89]. The precise pathological mechanism remains to be elucidated, but in healthy epithelial cells *CTNND1* binds to E-cadherin to stabilize adherens junctions and desmosomes, and therefore displacement of *CTNND1* causes endocytosis of *CDH1* and loss of the junction. Another possibility is disruption of the canonical WNT pathway signaling, as *CTNND1* is known to modulate transcription by binding to transcription factors such as Kaiso in the *Wnt* pathway[90,91]. It is known, and further supported by the evidence in this work, that alternatively spliced isoforms of *CTNND1* are differentially expressed in the epithelium and mesenchyme, and here we show that those distinct splicing patterns are dependent on *Esrp1/2* activity. However, it is not known how the alternatively spliced isoforms differ in function, alter embryonic and craniofacial morphogenesis, or contribute to disease. Thus, further studies into the functional differences between *CTNND1* isoforms are warranted and would provide insight into the disease etiology of BCD or the mechanism of the cleft palate from *ESRP* loss-of-function.

Methods

Animal husbandry and breeding

All animal experiments were performed in accordance with protocols approved by Massachusetts General Hospital Animal Care and Usage Committee, and the Children's Hospital of Philadelphia Institutional Animal Care and Use Committee (IACUC). Embryos were collected and raised in E3 Medium (5.0 mM NaCl, 0.17 mM KCl, 0.33 mM $CaCl_2$, 0.33 mM $MgSO_4$) containing 0.0001% Methylene blue at 28.5 °C.

Gene variant identification, sequence alignment, and variant effect prediction

The study population comes from multiple domestic and international sites where recruitment and phenotypic assessment occurred following institutional review board approval for the local recruitment site and the coordinating center (Emory University). Three WGS datasets of 759 OFC trios from the Gabriella Miller Kids First (GMKF) Research (dbGaP; European trios, dbGaP: phs001168.v2.p2; Colombian trios, dbGaP: phs001420.v1.p1; Taiwanese trios, dbGaP: phs000094.v1.p1) were filtered for variants in *ESRP1, ESRP2*, and *CTNND1* that were (1) heterozygous in the affected patient, (2) had a minor allele frequency no greater than 0.001 in any population in gnomAD or 1000 Genomes, and (3) had a variant consequence of missense, frameshift, stop-gain, splicing, or in-frame insertion/deletion. We further supplemented the resulting list with additional variants from ClinVar associated with an OFC or autosomal recessive deafness. In total, the ClinVar list included 12 *ESRP1* and 20 *ESRP2* variants. ClinVar variants were accessed in 2021, we note that new variants have been uploaded to ClinVar for ESRP1 and ESRP2, but these new variants did not include relevant clinical phenotype information so were not included in this study. OFC-associated genes were based on a previously published study that curated a list of approximately 500 genes based on known clinical syndromes and association results from GWAS[70].

To further refine the variant list to identify variants for testing in mouse and zebrafish assays, we aligned the human, mouse and zebrafish *Esrp1* and *Esrp2* amino acid sequences using Clustal Omega[92]. 7 *ESRP1* and 12 *ESRP2* variants at fully conserved residues were then annotated using SIFT, PolyPhen-2, and AlphaMissense to obtain the predicted change in protein function and were categorized as benign, pathogenic, or of unknown significance. We included a silent mutation from *ESRP2*, at threonine 475 (T475T) that served as an internal negative control. Variants were annotated to the following human transcripts: *ESRP1*: NM_017697.4/ENST00000433389.8; ESRP2: NM_024939.3/ENST00000473183.7; and *CTNND1*: NM_001085458.2/ENST00000399050.10.

All variants from this study are listed in Table 1 in the Supplementary material.

Rare-variants analysis

We performed rare variant burden tests using RV-TDT[2] for protein-altering variants in *ESRP1*, *ESRP2*, and *CTNND1* that had a minor allele frequency of less than 0.1% in any gnomAD population. DenovolyzeR (0.2.0), an *R* package which compares the observed number of DNMs to the expected number of DNMs based on a mutational model developed by Samocha et al. [93], was used to determine if de novo variants were enriched in these three genes.

Plasmid generation, site-directed mutagenesis, and mRNA synthesis

mRNA from wildtype zebrafish embryos was collected at multiple time points from 6 h post fertilization (hpf) to 4 days post fertilization (dpf), reverse transcribed, and combined to make pooled cDNA to clone the *esrp1* coding sequence (CDS). *esrp1* and *esrp2* were each cloned into a pCS2 + 8 plasmid backbone using the In-Fusion HD Cloning Kit (Clontech). The resulting pCS2 + 8-*esrp2* plasmid was mutagenized with synonymous mutations surrounding the translational start-site using the GeneArt SDM system (ThermoFisher) to generate *esrp2* transcripts resistant to *esrp2* morpholino binding. The 19 human *ESRP1* and *ESRP2* variants were each individually introduced to the pCS2 + 8-*esrp1* or MO-resistant pCS2 + 8-*esrp2* plasmids through the GeneArt SDM system. All generated pCS2 + 8 plasmids were digested with NotI at 37 °C for 1 h, and capped mRNA was synthesized using the SP6 mMessage mMachine kit (ThermoFisher).

For the murine Py2T transfection experiments, we used the pIBX-C-FF(B)-mCherry-*esrp1*(2 A)- + CKLP plasmid containing the mouse *Esrp1* cDNA sequence, fused to a mCherry tag (gift from Russ Carstens, University of Pennsylvania). Mouse *Esrp2* cDNA was purchased from Genomics Online. *Esrp1* cDNA was cloned into the pcDNA3.1 backbone containing a CMV promoter and SV40 polyA tailing sequence for expression in mammalian cells using the In-Fusion HD Cloning Kit (Clontech) to generate the *pcDNA3.1-esrp1-mCherry plasmid*. An mCherry tag was fused in-frame onto the *Esrp2* cDNA and introduced into the pcDNA3.1 backbone through a multi-insert in-Fusion cloning strategy, using the pIBX-C-FF(B)-mCherry-Esrp1(2 A)- + CKLP as the template for the 2A-mCherry sequence to generate the pcDNA3.1-*esrp2-mCherry plasmid*. Selected human *ESRP1* and *ESRP2* gene variants were introduced using the GeneArt SDM system, as described above.

Zebrafish microinjection and *esrp1/2* rescue assay

We previously generated a zebrafish line carrying homozygous loss-of-function alleles in *esrp1* through CRISPR/Cas9 harboring -4 bp indels which led to a frameshift mutation and early protein truncation[52]. *esrp2* morpholinos (GeneTools) were reconstituted to a concentration of 8 µg/uL in water and stored in single-use aliquots at RT. 2 nL droplets containing (1) 8 ng *esrp2* morpholino, (2) 0.05% phenol red and (3) 200 pg of *esrp1, esrp2*, or *esrp* gene-variant mRNA were microinjected directly into the cytoplasm of one-cell stage *esrp1*$^{-/-}$ zebrafish embryos and grown until 4 dpf (We have previously shown that the *esrp2* morpholino, injected into *esrp1*$^{-/-}$ *esrp2*$^{wt/wt}$ is sufficient to phenocopy the *esrp1*$^{-/-}$; *esrp2*$^{-/-}$ phenotype, which is consistent with previous descriptions[22,52]). Since all the injected embryos were derived from mating of *esrp1*$^{-/-}$ males and females, all animals had the *esrp1*$^{-/-}$ genotype and did not require additional genotyping after phenotype analysis. At 4 dpf, embryos were fixed in 4% formaldehyde, stained with acid-free Alcian blue as previously described[94], and micro-dissected to inspect the ANC. The ANC phenotype flatmount was then scored as wildtype ANC, cleft ANC or rescued ANC.

PY2T cell maintenance and transfection

Mouse Py2T cells and *Esrp1/2* DKO Py2T cells were a gift from Russ Carstens from the University of Pennsylvania[23]. Cells were maintained in DMEM supplemented with 10% FBS and penicillin/streptomycin and were not cultured past passage 30. 10.8 µg of plasmid was transfected onto 10^6 cells using the 100 µL Neon system (ThermoFisher) with a single, 30 s pulse at 1400 V and plated onto 6-well plates. Cells were harvested for RNA after 24 h, reverse transcribed, and the cDNA was used for RT-PCR using primers spanning the splice junctions for *Ctnnd1* exons 1 and 3 and *Afhgef11* exons 36 and 38, Arhgef11 Forward (TCAAGCTCAGAACCAG CAGGAAGT) and Arhgef11 Reverse (TGCTCGATGGTGTGGAA-GATCACA), as described[23]. The gels were quantified by densitometry using Fiji/ImageJ and the results are expressed as mean ± SEM. Statistical analysis involved using GraphPad Prism 9.0 for Windows. The experiments were performed in triplicate. One-way Anova test, with each comparison standing alone was used for statistical analysis. $P < 0.05$ was considered statistically significant.

ctnnd1 mRNA injection into *esrp1*$^{-/-}$; *esrp2*$^{+/-}$ intercross

To construct the mRNA in vitro transcription template, synthetic Ctnnd1 cDNA, isoform-201 on Ensembl (ENSDART00000106048.4), was cloned into the linearized DNA template vector (Takara Bio USA). The plasmid vectors were purified by a QIAprep spin miniprep kit (QIAGEN). The plasmid was digested with Hind III HF (NEB Biolabs) at 37 °C for 1 h, 80 °C for 20 m for inactivation and mRNA was synthesized using the T7 MEGAshortscript kit (ThermoFisher).

For micro-injection, progeny of *esrp1*$^{-/-}$; *esrp2*$^{+/-}$ inter-cross, previous described by Carroll, 2020[52] were injected at the single cell stage with either 250 pg of *ctnnd1* mRNA (along with water), or *gfp* mRNA, for controls. Injected embryos were raised to 4 dpf, at which time embryos were fixed in 4% formaldehyde, stained with acid-free Alcian blue, and microdissected to inspect the ANC. The ANC was scored as wildtype ANC or cleft ANC. Additionally, the pectoral fins were also analyzed and scored as wildtype fin or curled fin. For the otolith phenotype, wildtype was scored when the otoliths were separate and the mutant phenotype when the otoliths were fused. For the paired bilateral structures, if one fin was curled or one set of otoliths were fused, the animal was scored as mutant. After the phenotypic assessments for ANC, fin and otoliths, both the mRNA injected embryos and the control-injected embryos was tracked and individually genotyped. Whenever there is an animal with genotype of *esrp1*$^{-/-}$; *esrp2*$^{-/-}$ but exhibited ANC that are not fully cleft, fins that are not fully curled and separate otoliths, these animals were scored as rescues.

RNA in situ hybridization staining (RNAScope and BaseScope)

Wildtype and *esrp1*$^{-/-}$; *esrp2*$^{+/-}$ zebrafish were crossed and the progeny embryos raised to 4 dpf. The *esrp1*$^{-/-}$; *esrp2*$^{-/-}$ double mutant embryos were scored at 4 dpf based on the abrogated pectoral fin phenotype. The wild type and *esrp1*$^{-/-}$; *esrp2*$^{-/-}$ embryos were fixed in 4% formaldehyde, taken through a sucrose gradient, and then cryo embedded and sectioned. RNAScope probes were designed with assistance from ACDBio to target the region of 700–1661 base pairs of the RNA for DR Ctnnd1 XM_021476936.1, which corresponds to ENSDART00000106048.4 for ensemble 201.

Additionally, RNAScope and BaseScope probes were designed for murine Esrp1 (we have previously shown that Esrp1 and Esrp2 colocalize in the oral epithelium)[52]. Hybridization and staining were performed according to the manufacturer's protocol. Stained sections were imaged on a Leica SP8 confocal microscope where a Z-stack was obtained and analyzed on imageJ software to obtain optimal images. BaseScope probes were designed and purchased from ACDBio to specifically target the Ctnnd1 long and short isoforms. Staining was carried out according to the manufacturer's protocols on both fixed, frozen, and sectioned wildtype and Esrp1/2 DKO at E15. Stained sections were imaged as above.

Statistics and reproducibility

The results are expressed as percentage or as mean ± SEM. Statistical analysis was using GraphPad Prism 10 for Windows (GraphPad Software, San Diego, CA, www.graphpad.com). All experiments were performed at least in triplicate. Two-way analysis of variance or Student *t*-test was used for statistical analysis. $P < 0.05$ was considered statistically significant.

Reporting summary

Further information on research design is available in the Nature Portfolio Reporting Summary linked to this article.

Data availability

The authors declare that the data supporting the findings of this study are available within the paper and its supplementary information files (Supplementary data 1). Any other information that supports the findings of this study are available on request from the corresponding author, ECL.

Received: 15 February 2024; Accepted: 9 August 2024;
Published online: 23 August 2024

References

1. Bishop, M. R. et al. Genome-wide enrichment of de novo coding mutations in orofacial cleft trios. *Am. J. Hum. Genet.* **107**, 124–136 (2020).
2. Bureau, A. et al. Whole exome sequencing of distant relatives in multiplex families implicates rare variants in candidate genes for oral clefts. *Genetics* **197**, 1039–1044 (2014).
3. Carlson, J. C. et al. Identifying genetic sources of phenotypic heterogeneity in orofacial clefts by targeted sequencing. *Birth Defects Res.* **109**, 1030–1038 (2017).
4. Leslie, E. J. Genetic models and approaches to study orofacial clefts. *Oral Dis*. https://doi.org/10.1111/odi.14109 (2021).
5. Mukhopadhyay, N. et al. Genome-wide association study of non-syndromic orofacial clefts in a multiethnic sample of families and controls identifies novel regions. *Front. Cell Dev. Biol.* **9**, 621482 (2021).
6. Beaty, T. H., Marazita, M. L. & Leslie, E. J. Genetic factors influencing risk to orofacial clefts: today's challenges and tomorrow's opportunities. *F1000Research* **5**, 2800 (2016).
7. Dixon, M. J., Marazita, M. L., Beaty, T. H. & Murray, J. C. Cleft lip and palate: understanding genetic and environmental influences. *Nat. Rev. Genet.* **12**, 167–178 (2011).
8. Welzenbach, J. et al. Integrative approaches generate insights into the architecture of non-syndromic cleft lip with or without cleft palate. *HGG Adv.* **2**, 100038 (2021).
9. Carlson, J. C. et al. A systematic genetic analysis and visualization of phenotypic heterogeneity among orofacial cleft GWAS signals. *Genet. Epidemiol.* **43**, 704–716 (2019).

10. Curtis, S. W. et al. The PAX1 locus at 20p11 is a potential genetic modifier for bilateral cleft lip. *HGG Adv.* **2,** (2021).
11. Takahashi, M. et al. Whole-genome sequencing in a pair of monozygotic twins with discordant cleft lip and palate subtypes. *Oral. Dis.* **24**, 1303–1309 (2018).
12. Richardson, R. et al. p63 exerts spatio-temporal control of palatal epithelial cell fate to prevent cleft palate. *PLoS Genet.* **13**, e1006828 (2017).
13. Ferretti, E. et al. A conserved Pbx-Wnt-p63-Irf6 regulatory module controls face morphogenesis by promoting epithelial apoptosis. *Dev. Cell* **21**, 627–641 (2011).
14. Kondo, S. et al. Mutations in IRF6 cause Van der Woude and popliteal pterygium syndromes. *Nat. Genet.* **32**, 285–289 (2002).
15. Ingraham, C. R. et al. Abnormal skin, limb and craniofacial morphogenesis in mice deficient for interferon regulatory factor 6 (Irf6). *Nat. Genet.* **38**, 1335–1340 (2006).
16. Richardson, R. J. et al. Irf6 is a key determinant of the keratinocyte proliferation-differentiation switch. *Nat. Genet.* **38**, 1329–1334 (2006).
17. de la Garza, G. et al. Interferon regulatory factor 6 promotes differentiation of the periderm by activating expression of Grainyhead-like 3. *J. Investig. Dermatol.* **133**, 68–77 (2013).
18. Peyrard-Janvid, M. et al. Dominant mutations in GRHL3 cause Van der Woude Syndrome and disrupt oral periderm development. *Am. J. Hum. Genet.* **94**, 23–32 (2014).
19. Alharatani, R. et al. Novel truncating mutations in CTNND1 cause a dominant craniofacial and cardiac syndrome. *Hum. Mol. Genet.* **29**, 1900–1921 (2020).
20. Cox, L. L. et al. Mutations in the epithelial cadherin-p120-catenin complex cause mendelian non-syndromic cleft lip with or without cleft palate. *Am. J. Hum. Genet.* **102**, 1143–1157 (2018).
21. Bebee, T. W. et al. The splicing regulators Esrp1 and Esrp2 direct an epithelial splicing program essential for mammalian development. *Elife* **4,** e08954 (2015).
22. Burguera, D. et al. Evolutionary recruitment of flexible Esrp-dependent splicing programs into diverse embryonic morphogenetic processes. *Nat. Commun.* **8**, 1799 (2017).
23. Lee, S. et al. Esrp1-regulated splicing of Arhgef11 isoforms is required for epithelial tight junction integrity. *Cell Rep.* **25**, 2417–2430.e2415 (2018).
24. Yang, Y. & Carstens, R. P. Alternative splicing regulates distinct subcellular localization of epithelial splicing regulatory protein 1 (Esrp1) isoforms. *Sci. Rep.* **7**, 3848 (2017).
25. Adzhubei, I. A. et al. A method and server for predicting damaging missense mutations. *Nat. Methods* **7**, 248–249 (2010).
26. Choi, Y., Sims, G. E., Murphy, S., Miller, J. R. & Chan, A. P. Predicting the functional effect of amino acid substitutions and indels. *PLoS One* **7**, e46688 (2012).
27. Kumar, P., Henikoff, S. & Ng, P. C. Predicting the effects of coding non-synonymous variants on protein function using the SIFT algorithm. *Nat. Protoc.* **4**, 1073–1081 (2009).
28. Reva, B., Antipin, Y. & Sander, C. Predicting the functional impact of protein mutations: application to cancer genomics. *Nucleic Acids Res.* **39**, e118 (2011).
29. Tang, H. & Thomas, P. D. Tools for predicting the functional impact of nonsynonymous genetic variation. *Genetics* **203**, 635–647 (2016).
30. Liu, X., Li, C., Mou, C., Dong, Y. & Tu, Y. dbNSFP v4: a comprehensive database of transcript-specific functional predictions and annotations for human nonsynonymous and splice-site SNVs. *Genome Med.* **12**, 103 (2020).
31. Frazer, J. et al. Disease variant prediction with deep generative models of evolutionary data. *Nature* **599**, 91–95 (2021).
32. Oliver, J. D. et al. Molecular diagnostics and in utero therapeutics for orofacial clefts. *J. Dent. Res.***99**, 1221–1227 (2020).
33. Richards, S. et al. Standards and guidelines for the interpretation of sequence variants: a joint consensus recommendation of the American College of Medical Genetics and Genomics and the Association for Molecular Pathology. *Genet. Med.* **17**, 405–424 (2015).
34. Bean, L. J. H. et al. Diagnostic gene sequencing panels: from design to report—a technical standard of the American College of Medical Genetics and Genomics (ACMG). *Genet. Med.* **22**, 453–461 (2020).
35. Jaravine, V. et al. Annotation of human exome gene variants with consensus pathogenicity. *Genes* **11,** https://doi.org/10.3390/genes11091076 (2020).
36. Harnish, J. M., Deal, S. L., Chao, H. T., Wangler, M. F. & Yamamoto, S. In vivo functional study of disease-associated rare human variants using Drosophila. *J. Vis. Exp*. https://doi.org/10.3791/59658 (2019).
37. Wang, J., Liu, Z., Bellen, H. J. & Yamamoto, S. Navigating MARRVEL, a web-based tool that integrates human genomics and model organism genetics information. *J. Vis. Exp*. https://doi.org/10.3791/59542 (2019).
38. Raud, L. et al. Functional analysis of novel RHD variants: splicing disruption is likely to be a common mechanism of variant D phenotype. *Transfusion* **59**, 1367–1375 (2019).
39. Schaid, D. J., Chen, W. & Larson, N. B. From genome-wide associations to candidate causal variants by statistical fine-mapping. *Nat. Rev. Genet.* **19**, 491–504 (2018).
40. Li, E. B. et al. Rapid functional analysis of computationally complex rare human IRF6 gene variants using a novel zebrafish model. *PLoS Genet.* **13**, e1007009 (2017).
41. Kim, S. S. et al. Improving the informativeness of Mendelian disease-derived pathogenicity scores for common disease. *Nat. Commun.* **11**, 6258 (2020).
42. Itan, Y. et al. The mutation significance cutoff: gene-level thresholds for variant predictions. *Nat. Methods* **13**, 109–110 (2016).
43. Liu, Y., Yeung, W. S. B., Chiu, P. C. N. & Cao, D. Computational approaches for predicting variant impact: an overview from resources, principles to applications. *Front. Genet.* **13**, 981005 (2022).
44. Zhang, M. et al. Functional characterization of a novel IRF6 frameshift mutation from a Van Der Woude syndrome family. *Front. Genet.* **11**, 562 (2020).
45. Griesemer, D. et al. Genome-wide functional screen of 3'UTR variants uncovers causal variants for human disease and evolution. *Cell* **184**, 5247–5260.e5219 (2021).
46. Findlay, G. M. et al. Accurate classification of BRCA1 variants with saturation genome editing. *Nature* **562**, 217–222 (2018).
47. Glazer, A. M. et al. High-throughput reclassification of SCN5A variants. *Am. J. Hum. Genet.* **107**, 111–123 (2020).
48. Giacomelli, A. O. et al. Mutational processes shape the landscape of TP53 mutations in human cancer. *Nat. Genet.* **50**, 1381–1387 (2018).
49. Mighell, T. L., Evans-Dutson, S. & O'Roak, B. J. A saturation mutagenesis approach to understanding PTEN lipid phosphatase activity and genotype-phenotype relationships. *Am. J. Hum. Genet.* **102**, 943–955 (2018).
50. Jia, X. et al. Massively parallel functional testing of MSH2 missense variants conferring Lynch syndrome risk. *Am. J. Hum. Genet.* **108**, 163–175 (2021).
51. Warzecha, C. C., Sato, T. K., Nabet, B., Hogenesch, J. B. & Carstens, R. P. ESRP1 and ESRP2 are epithelial cell-type-specific regulators of FGFR2 splicing. *Mol. Cell* **33**, 591–601 (2009).
52. Carroll, S. H. et al. An Irf6-Esrp1/2 regulatory axis controls midface morphogenesis in vertebrates. *Development* **147**, dev194498 (2020).
53. Lee, S. et al. Cleft lip and cleft palate in Esrp1 knockout mice is associated with alterations in epithelial-mesenchymal crosstalk. *Development* **147**, https://doi.org/10.1242/dev.187369 (2020).
54. Schilling, T. F. & Kimmel, C. B. Musculoskeletal patterning in the pharyngeal segments of the zebrafish embryo. *Development* **124**, 2945–2960 (1997).
55. Wada, N. et al. Hedgehog signaling is required for cranial neural crest morphogenesis and chondrogenesis at the midline in the zebrafish skull. *Development* **132**, 3977–3988 (2005).

56. Dougherty, M. et al. Distinct requirements for wnt9a and irf6 in extension and integration mechanisms during zebrafish palate morphogenesis. *Development* **140**, 76–81 (2013).
57. Swartz, M. E., Sheehan-Rooney, K., Dixon, M. J. & Eberhart, J. K. Examination of a palatogenic gene program in zebrafish. *Dev. Dyn.* **240**, 2204–2220 (2011).
58. Rohacek, A. M. et al. ESRP1 mutations cause hearing loss due to defects in alternative splicing that disrupt cochlear development. *Dev. Cell* **43**, 318–331.e315 (2017).
59. Freytag, M. et al. Epithelial splicing regulatory protein 1 and 2 (ESRP1 and ESRP2) upregulation predicts poor prognosis in prostate cancer. *BMC Cancer* **20**, 1220 (2020).
60. Peart, N. J. et al. The global Protein-RNA interaction map of ESRP1 defines a post-transcriptional program that is essential for epithelial cell function. *iScience* **25**, 105205 (2022).
61. Panizzi, J. R., Jessen, J. R., Drummond, I. A. & Solnica-Krezel, L. New functions for a vertebrate Rho guanine nucleotide exchange factor in ciliated epithelia. *Development* **134**, 921–931 (2007).
62. Warzecha, C. C., Shen, S., Xing, Y. & Carstens, R. P. The epithelial splicing factors ESRP1 and ESRP2 positively and negatively regulate diverse types of alternative splicing events. *RNA Biol.* **6**, 546–562 (2009).
63. Itoh, M., Radisky, D. C., Hashiguchi, M. & Sugimoto, H. The exon 38-containing ARHGEF11 splice isoform is differentially expressed and is required for migration and growth in invasive breast cancer cells. *Oncotarget* **8**, 92157–92170 (2017).
64. Shapiro, I. M. et al. An EMT-driven alternative splicing program occurs in human breast cancer and modulates cellular phenotype. *PLoS Genet.* **7**, e1002218 (2011).
65. Landrum, M. J. et al. ClinVar: improvements to accessing data. *Nucleic Acids Res.* **48**, D835–D844 (2020).
66. Sayers, E. W. et al. Database resources of the National Center for Biotechnology Information. *Nucleic Acids Res.* **49**, D10–D17 (2021).
67. Mukhopadhyay, N. et al. Whole genome sequencing of orofacial cleft trios from the Gabriella Miller Kids First Pediatric Research Consortium identifies a new locus on chromosome 21. *Hum. Genet.* **139**, 215–226 (2020).
68. Cheng, J. et al. Accurate proteome-wide missense variant effect prediction with AlphaMissense. *Science* **381**, eadg7492 (2023).
69. Faux, M. C. et al. APC regulation of ESRP1 and p120-catenin isoforms in colorectal cancer cells. *Mol. Biol. Cell* **32**, 120–130 (2021).
70. Diaz Perez, K. K. et al. Rare variants found in clinical gene panels illuminate the genetic and allelic architecture of orofacial clefting. *Genet. Med.* **25**, 100918 (2023).
71. Kievit, A. et al. Variants in members of the cadherin-catenin complex, CDH1 and CTNND1, cause blepharocheilodontic syndrome. *Eur. J. Hum. Genet.* **26**, 210–219 (2018).
72. Davis, M. A., Ireton, R. C. & Reynolds, A. B. A core function for p120-catenin in cadherin turnover. *J. Cell Biol.* **163**, 525–534 (2003).
73. Fukumoto, Y., Shintani, Y., Reynolds, A. B., Johnson, K. R. & Wheelock, M. J. The regulatory or phosphorylation domain of p120 catenin controls E-cadherin dynamics at the plasma membrane. *Exp. Cell Res.* **314**, 52–67 (2008).
74. Ireton, R. C. et al. A novel role for p120 catenin in E-cadherin function. *J. Cell Biol.* **159**, 465–476 (2002).
75. Ishiyama, N. et al. Dynamic and static interactions between p120 catenin and E-cadherin regulate the stability of cell-cell adhesion. *Cell* **141**, 117–128 (2010).
76. Reynolds, A. B. et al. Identification of a new catenin: the tyrosine kinase substrate p120cas associates with E-cadherin complexes. *Mol. Cell Biol.* **14**, 8333–8342 (1994).
77. Reynolds, A. B., Daniel, J. M., Mo, Y. Y., Wu, J. & Zhang, Z. The novel catenin p120cas binds classical cadherins and induces an unusual morphological phenotype in NIH3T3 fibroblasts. *Exp. Cell Res.* **225**, 328–337 (1996).
78. Schackmann, R. C., Tenhagen, M., van de Ven, R. A. & Derksen, P. W. p120-catenin in cancer - mechanisms, models and opportunities for intervention. *J. Cell Sci.* **126**, 3515–3525 (2013).
79. Stairs, D. B. et al. Deletion of p120-catenin results in a tumor microenvironment with inflammation and cancer that establishes it as a tumor suppressor gene. *Cancer Cell* **19**, 470–483 (2011).
80. Overhoff, J. et al. Refinement of the 8q22.1 microdeletion critical region associated with Nablus mask-like facial syndrome. *Am. J. Med. Genet. A* **164A**, 259–263 (2014).
81. Yu, Y. et al. Genome-wide analyses of non-syndromic cleft lip with palate identify 14 novel loci and genetic heterogeneity. *Nat. Commun.* **8**, 14364 (2017).
82. Lin-Shiao, E. et al. p63 establishes epithelial enhancers at critical craniofacial development genes. *Sci. Adv.* **5**, eaaw0946 (2019).
83. Griffin, C. & Saint-Jeannet, J. P. Spliceosomopathies: diseases and mechanisms. *Dev. Dyn.* **249**, 1038–1046 (2020).
84. Dennison, B. J. C., Larson, E. D., Fu, R., Mo, J. & Fantauzzo, K. A. Srsf3 mediates alternative RNA splicing downstream of PDGFRalpha signaling in the facial mesenchyme. *Development* **148,** dev199448 (2021).
85. Timberlake, A. T. et al. Haploinsufficiency of SF3B2 causes craniofacial microsomia. *Nat. Commun.* **12**, 4680 (2021).
86. McDonald, E. F., Oliver, K. E., Schlebach, J. P., Meiler, J. & Plate, L. Benchmarking AlphaMissense pathogenicity predictions against cystic fibrosis variants. *PloS one*, **19**, e0297560 (2024).
87. Murali, H., Wang, P., Liao, E. C. & Wang, K. Genetic variant classification by predicted protein structure: a case study on IRF6. *Comput. Struct. Biotechnol. J.* **23**, 892–904 (2024).
88. Dominguez, C., Fisette, J. F., Chabot, B. & Allain, F. H. Structural basis of G-tract recognition and encaging by hnRNP F quasi-RRMs. *Nat. Struct. Mol. Biol.* **17**, 853–861 (2010).
89. Ghoumid, J. et al. Blepharocheilodontic syndrome is a CDH1 pathway-related disorder due to mutations in CDH1 and CTNND1. *Genet. Med.* **19**, 1013–1021 (2017).
90. Del Valle-Perez, B. et al. Wnt controls the transcriptional activity of Kaiso through CK1epsilon-dependent phosphorylation of p120-catenin. *J. Cell Sci.* **124**, 2298–2309 (2011).
91. Park, J. I. et al. Kaiso/p120-catenin and TCF/beta-catenin complexes coordinately regulate canonical Wnt gene targets. *Dev. cell* **8**, 843–854 (2005).
92. Sievers, F. & Higgins, D. G. The clustal omega multiple alignment package. *Methods Mol. Biol.* **2231**, 3–16 (2021).
93. Samocha, K. E. et al. A framework for the interpretation of de novo mutation in human disease. *Nat. Genet.* **46**, 944–950 (2014).
94. Walker, M. B. & Kimmel, C. B. A two-color acid-free cartilage and bone stain for zebrafish larvae. *Biotech. Histochem.* **82**, 23–28 (2007).

Acknowledgements

We thank the Aquatics Core at Massachusetts General Hospital and Children's Hospital of Philadelphia (CHOP) for their dedication to fish health and the maintenance of our colonies. We thank the CHOP IDDRC Biostatistics and Data Science core (HD105354) for consultation. We are grateful for the funding support from the National Institutes of Health (HG013031) to K.W. and (DE032332, DE027983) to E.C.L., research and fellowship grants from Shriners Hospitals for Children and institutional support from Children's Hospital of Philadelphia.

Author contributions

Study conception and design: CCS, CMT, JM, ECL. Data collection: CCS, CMT, JM, CT, ED, SHC. Contributed data and analysis tools: CCS, CMT, HM, SHC SK, SWC, CHEC, FW, EK, RPC, YX, KW, EJL, ECL. Paper preparation: CCS, CMT, JM, RPC, KW, EJL, ECL.

Competing interests

The authors declare no competing interests.

Additional information

Supplementary information The online version contains supplementary material available at https://doi.org/10.1038/s42003-024-06715-3.

Correspondence and requests for materials should be addressed to Eric C. Liao.

Peer review information *Communications Biology* thanks Auinash Kalsotra, Walid Fakhouri, and Lorena E. Maili for their contribution to the peer review of this work. Primary Handling Editor: Christina Karlsson Rosenthal. A peer review file is available.